Water-COOH Composite Structure with Enhanced Hydrophobicity Formed by Water Molecules Embedded into Carboxyl-Terminated Self-Assembled Monolayers

Pan Guo,[1,2] Yusong Tu,[3,*] Jinrong Yang,[1,2] Chunlei Wang,[1] Nan Sheng,[1] and Haiping Fang[1,†]
[1]Division of Interfacial Water and Key Laboratory of Interfacial Physics and Technology, Shanghai Institute of Applied Physics, Chinese Academy of Sciences, Shanghai 201800, China
[2]University of Chinese Academy of Sciences, Beijing 100049, China
[3]College of Physics Science and Technology, Yangzhou University, Jiangsu 225009, China
(Received 11 March 2015; revised manuscript received 7 August 2015; published 28 October 2015)

By combining molecular dynamics simulations and quantum mechanics calculations, we show the formation of a composite structure composed of embedded water molecules and the COOH matrix on carboxyl-terminated self-assembled monolayers (COOH SAMs) with appropriate packing densities. This composite structure with an integrated hydrogen bond network inside reduces the hydrogen bonds with the water above. This explains the seeming contradiction on the stability of the surface water on COOH SAMs observed in experiments. The existence of the composite structure at appropriate packing densities results in the two-step distribution of contact angles of water droplets on COOH SAMs, around 0° and 35°, which compares favorably to the experimental measurements of contact angles collected from forty research articles over the past 25 years. These findings provide a molecular-level understanding of water on surfaces (including surfaces on biomolecules) with hydrophilic functional groups.

DOI: 10.1103/PhysRevLett.115.186101 PACS numbers: 68.08.Bc, 61.20.Ja, 61.30.Hn, 87.90.+y

Carboxyl-terminated self-assembled monolayers (COOH SAMs) have been of wide interest owing to their extensive applications in nanoscience and nanotechnology [1–9]. However, even after 25 years of study, COOH SAMs continue to present puzzling observations. Experimental values of contact angles of water droplets on COOH SAMs collected from forty research articles have ranged from 0° to 50° [2,10–14]. Although COOH SAMs were found to have higher water desorption energy than hydroxyl-terminated SAMs (OH SAMs) and amide-terminated SAMs (CONH2 SAMs) at very low coverage of water in temperature-programmed desorption experiments [15,16], Raman spectral data revealed even less stability of the nanoscale interfacial water on COOH SAM than that on OH SAM [17]. Moreover, COOH SAM was found to present abnormal coverage-dependent kinetics of water desorption [16]. Recently, James *et al.* reported the presence of nanoscale water droplets on top of a continuous few-angstrom-thin water layer on COOH SAM by using x-ray, neutron reflectometry, and atomic force microscopy (AFM) methods [14]. Unfortunately, the physical nature behind these seemingly contradictory results is still unclear, although there have been some theoretical attempts [18–22]. In addition, both experiments [8,23,24] and molecular dynamics (MD) simulations [21] have shown that COOH SAMs exhibited *p*H-dependent contact angles owing to the hydrogen bonding of COOH groups mainly to interfacial water at low *p*H but to each other at high *p*H. However, most of the contact angle measurements used distilled or deionized water. Thus the impact of *p*H cannot explain the widely differing measurements of the contact angle.

Here, by combining MD simulations with quantum mechanics calculations, we have unraveled these elusive phenomena of water on COOH SAMs. We have attributed the essential physics of this system to the formation of embedded-water–COOH composite structures in which water molecules are embedded into the COOH matrix on COOH SAMs. The presence of embedded water and of the integrated hydrogen bonding (H-bond) network in the composite structure explains the abnormal increase of water desorption energy on COOH SAM under conditions of decreasing water coverage, even down to 4% [16], and also accounts for the decreased stabilization of interfacial water on COOH SAM as compared to that on OH SAM [17]. It should be noted that it is just the water molecules themselves that actively stabilize the composite structure constituted by embedded water and the COOH matrix; meanwhile, the stable anhydrous COOH matrix falls into different conformations, based on the quantum mechanics computations. The relevant contact angles of water on COOH SAMs, along with the related stability of the composite structure, were found to exhibit two states, at either ∼0° or ∼35° in our simulations, which compared favorably to the experimental measurements of contact angles collected from forty research articles over the past 25 years [2,10–14]. Our findings provide a molecular-level understanding of water on COOH SAMs and many other surfaces with hydrophilic groups, offering a guide for various relevant applications and may provide new insights into understanding the behavior of water on biological macromolecules.

The COOH SAMs were constructed with four-carbon-long alkyl chains, which have attached at one end to COOH

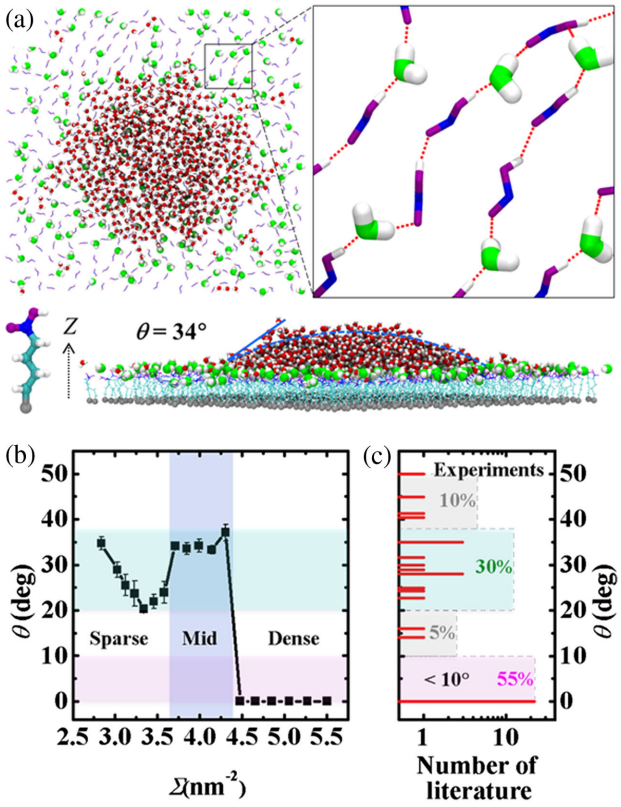

FIG. 1 (color online). (a) The four-carbon-long alkyl chain modified with a COOH group, together with top and side view snapshots of water on COOH SAM with a packing density of $\Sigma = 4.00\ \mathrm{nm}^{-2}$ (model atoms, gray; COOH groups, blue, purple and white; water, red and white; embedded water, green and white; alkyl chains, blue lines in side view, but omitted for clear views in the top view; H bonds, red dashed lines). (b) Contact angle θ of water droplets on COOH SAMs as a function of Σ. The midrange is marked as light blue. (c) Contact angle values of water on COOH SAMs, as measured from experiments over its numbers achieved in all the references we found (for literature citations, see Table S3 in the Supplemental Material [28]). 85% (34/40) fell into two ranges, i.e., 22 of them were less than 10° (light red) and 12 of them, ~30° (light green).

groups that being exposed to water [Fig. 1(a)]. The other end is attached to a layer of model atoms position restrained by harmonic springs at locations consistent with those on a 111 surface of an FCC lattice. We varied the packing density (Σ) from $5.50\ \mathrm{nm}^{-2}$ to $2.84\ \mathrm{nm}^{-2}$. For each packing density, we employed quantum mechanics calculations to optimize the structures of COOH SAMs with and without water in its smallest repeating unit [Fig. 2(a)], with the PBE GGA functional [25] in the Dmol3 [26,27] module of the Materials Studio package, in conjunction with the double numeric plus polarization (DNP) basis set. An all-electron atomic basis set was applied for the core electrons (see detailed quantum mechanics methods in the Supplemental Material [28]). MD simulations were carried out to calculate contact angles of water droplets on COOH SAMs (see Fig. S1 in the Supplemental Material [28]).

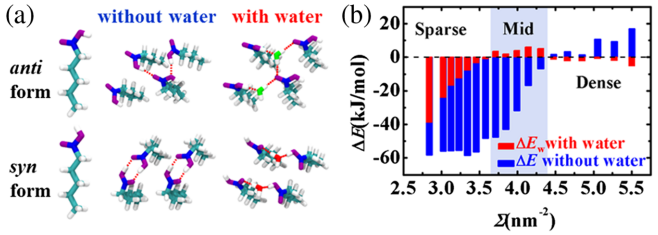

FIG. 2 (color online). Geometry optimized structures of COOH SAM and its stability. (a) Top view of the most stable geometry optimized structures of COOH SAM without and with water molecules at $\Sigma = 4.00\ \mathrm{nm}^{-2}$ for anti- (upper) and syn-form (lower) structures. All color settings are the same as in Fig. 1(a). (b) Energy difference, $\Delta E = E_{\mathrm{syn}} - E_{\mathrm{anti}}$ without water and $\Delta E_w = E_{\mathrm{syn},w} - E_{\mathrm{anti},w}$ with water at different values of Σ. The midrange with $\Delta E_w > 0$ is marked by light blue.

Initially, the COOH SAM with surface area of around $95.00\ \mathrm{nm}^2$ (x-y plane) was covered completely by a thin slab of water, where ~900 water molecules were used in the midrange of packing density Σ, and ~550 water molecules were used in the dense and sparse ranges (see Table S1 in the Supplemental Material [28]). The simulation time was 20 ns, and the data of the last 2 ns were collected for analysis. The periodic boundary condition was applied in all directions for all calculations. MD simulations were performed using a time step of 1.0 fs with Gromacs 4.5.1 [74] in the NVT ensemble with a velocity-rescale thermostat at a temperature of 300 K. The OPLSAA force field [75] was used for COOH SAM, and only its COOH dihedral parameters were modified to simply retain one form of COOH, i.e., the *anti* or *syn* form, which was a choice based on our quantum calculations (see Table S2 in Supplemental Material [28]). The SPC/E model [76] was used for the water molecules. The Particle-Mesh Ewald (PME) [77] method was adopted for the long-range electrostatic interactions with a cutoff of 1.2 nm, whereas a 1.2 nm cutoff was applied to the van der Waals interactions.

Figure 1(a) shows a typical view of water on COOH SAM with the packing density of $\Sigma = 4.00\ \mathrm{nm}^{-2}$. Remarkably, we observed not only a water droplet with the contact angle (denoted as θ) of ~34°, but also water molecules outside of the droplet on the COOH SAM [Fig. 1(a)]. Extensive examination showed that most of those outside water molecules had strong interaction with COOH SAM, with energy ≤ -50 kJ/mol. This type of water molecule was also found under the droplet, and the average energy and lifetimes of the H bonds between them and COOH were -41 ± 6 kJ/mol and 64 ± 3 ps, respectively, which were around 2 times stronger and 6 times longer than the corresponding values of the H bonds in the droplet (-20 ± 6 kJ/mol and 10 ± 2 ps; see Fig. S4 and Fig. S5 in the Supplemental Material [28]). Obviously, those water molecules were distinct from water molecules within the droplet. We termed the water molecules having a

water-SAM interaction energy ≤ -50 kJ/mol as embedded water, and the composition, which included both embedded water and the COOH matrix, was termed as the embedded-water–COOH composite structure. For the COOH SAM of $\Sigma = 4.00$ nm^{-2}, the average number of embedded water molecules per square nanometer (denoted as η) was $\sim$2.0 nm^{-2} [see Fig. 3(a)], much lower than that observed in a layer of water completely covering a flat solid surface ($\sim$9.5 nm^{-2}). We noted that, generally, there was only a water layer without any water droplets on the superhydrophilic surfaces. Water droplets were found to be stable on the ordered water monolayer on solid surfaces [78–82], but in this case, the surface was not solid since the COOH-terminated alkyl chains were flexible.

The water molecules themselves stabilized the embedded-water–COOH composite structure. The COOH functional group can have two types of configurations, i.e., the anti and syn form [see Fig. 2(a)]. These two configurations had not been taken into account in past studies of COOH SAMs, although the anti- and syn-form configurations had been discussed in investigations related to formic acid [83], acetic acid [84], and carboxylate [85], etc. In general classical MD simulations, the syn form is stable. Indeed, our quantum mechanics calculations on the anhydrous COOH SAM at $\Sigma = 4.00$ nm^{-2} also showed that the syn form was stable. Interestingly, if we applied quantum mechanics calculations to the system including both COOH SAM and water, the antiform of COOH SAM with embedded water was stabilized, as indicated by the most stable geometry optimized structures of COOH-SAMs with or without water embedded [Fig. 2(a)] (see also Table S5 and Table S6 in the Supplemental Material [28]). The antiform structure without water exhibited a higher energy of 32 kJ/mol than the syn form structure. Remarkably, a significant difference occurred when water was included. The antiform structure became more stable and had a lower energy of 4 kJ/mol than the syn-form structure. Therefore, "water is active" [86] to participate in the arrangement of the surface which stabilizes the composition of the antiform of COOH SAM and water, and the embedded-water–COOH composite structure therefore takes shape.

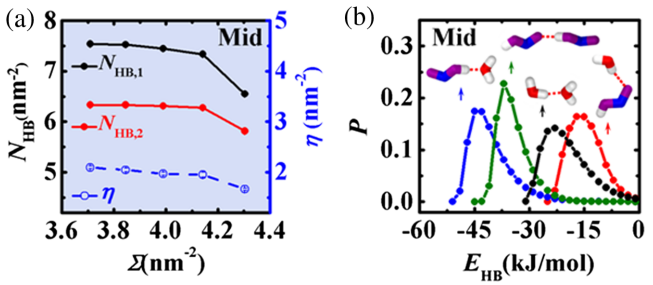

FIG. 3 (color online). (a) Average number of H bonds between the COOH matrix and water molecules within the region covered by water droplets ($N_{HB,1}$, black), and between the embedded-water–COOH composite structure and the water droplet above the composite structure ($N_{HB,2}$, red), together with the average number of embedded water molecules (η, blue, right blue axis), as a function of Σ in the midrange. (b) Energy distributions of four kinds of typical H bonds in the midrange. All atom-color settings are the same as Fig. 1(a).

The energy difference of the geometry optimized structures between anti- and syn-form structures (denoted as ΔE_w and ΔE for COOH SAM with and without water, respectively) is indicative of their stability, and their dependence on chain density Σ is demonstrated in Fig. 2(b). Here, $\Delta E_w = E_{syn,w} - E_{anti,w}$ and $\Delta E = E_{syn} - E_{anti}$, where $E_{anti,w}$ ($E_{syn,w}$) and E_{anti} (E_{syn}) are the system energies of the geometry optimized structures of the anti (syn) form COOH SAM, with and without water embedded, respectively. Σ can be divided into three ranges, i.e., sparse, mid, and dense ranges, in terms of the stability of antiform structures with water. In the midrange, ΔE_w are positive, showing that the antiform structures dominate. In both dense and sparse ranges, ΔE_w becomes negative, suggesting that syn-form structures dominate in these two ranges (see Fig. S7 in the Supplemental Material [28]).

We carried out MD simulations of water droplets on COOH SAMs, with only the dominant stable configuration form; the other form was overlooked for simplification (see detailed discussions in PS11 of the Supplemental Material [28]). Figure 1(b) shows contact angles (θ) of water droplets on COOH SAMs as a function of Σ. The θ shows an angle plateau of $\sim$35° in the midrange, and a value $\sim$0° in the dense range. In the sparse range, θ initially decreased and then increased slightly as Σ increased. Careful examination showed that the increase in contact angle was caused by the formation of more H bonds between COOHs within the COOH matrix (see Fig. S8 in the Supplemental Material [28]).

Interestingly, this two-step distribution of the contact angle compares favorably to the behavior of the experimentally measured contact angles reported in 40 research articles over the past 25 years. We noted that 85% (34/40) of the experimentally measured contact angles fell into two ranges, i.e., 22 of them were less than 10° and 12 of them, $\sim$30° [Fig. 1(c)]. Unfortunately, we could not directly compare each individual simulated contact angle value with the experimental results because most of the experiments did not report the details of packing densities of the COOH SAMs.

Furthermore, we show how the existence of the embedded water enhances the surface hydrophobicity in the midrange of Σ. We have calculated the average number of H bonds between the COOH matrix and the water molecules within the region covered by water droplets ($N_{HB,1}$), and between the embedded-water–COOH composite structure and the water droplet above ($N_{HB,2}$). Figure 3(a) presents $N_{HB,1}$ and $N_{HB,2}$, as the function of Σ. Obviously, $N_{HB,2}$ ($\sim$6.2 nm^{-2}) is less than $N_{HB,1}$ ($\sim$7.3 nm^{-2}). The reduced H-bonding number indicates a weak interaction between the composite

structure and the water droplet above the composite structure, which enhances the hydrophobicity of COOH SAM. The hydrophobicity enhancement effect of the embedded-water–COOH composite structure has a physical mechanism that is similar to the phenomenon of "ordered water monolayer that does not completely wet water" predicted recently [78]. However, here, the embedded water with the COOHs provides a weaker interaction with the water molecules above.

In order to sufficiently stabilize the embedded water, the water molecules should have strong H bonds with the COOH matrix and the composition of the embedded water and COOH matrix should be able to maintain an integrated H-bond network. As shown in Fig. 3(b), both the H bond between water and COOH ($\mathrm{H\text{-}\overset{H}{O}\cdots HO\text{-}C=O}$, $\cdots$ denotes H bond, with an average energy of -41 ± 6 kJ/mol) and the H bond between COOHs ($\mathrm{HO\text{-}C=O\cdots HO\text{-}C=O}$, with an average energy of -34 ± 4 kJ/mol) are much stronger than typical H bonds between water molecules (-20 ± 6 kJ/mol). Thus, we expect a dominant H-bonded structure: $\mathrm{H\text{-}\overset{H}{O}\cdots HO\text{-}C=O\cdots HO\text{-}C=O}$ in the integrated H-bond network; Fig. 1(a) displays this typical configuration of a H-bond network. This configuration consists mainly of structures with this dominant H-bond structure linked with one another, end to end, and also partial weak or bifurcated H bonds from the other suspended hydrogen atom of water. Therefore, the average number of H bonds formed by an embedded water molecule with COOHs reaches ~2.1 (Fig. S6 in the Supplemental Material [28]), and the ratio of embedded water to COOH in the integrated H-bond network is 1:2. That result is consistent with our quantum mechanics calculations [Fig. 2(b)]. Clearly, in the dense range there is not enough space for either water molecules to embed into the COOH matrix or for the formation of H bonds between COOHs, and thus the COOH SAM is completely wet [Fig. 1(b)]. In the sparse range, there are not enough COOHs to maintain an integrated H-bond network, and COOHs prefer to form localized cyclic H-bonded structures (see Fig. S7 in the Supplemental Material [28]).

The existence of embedded water and an integrated H-bond network in the composite structure also explains other puzzling observations. In an earlier study, the strong H bonds between embedded water and the COOH matrix in the intergraded H-bond network led to the abnormal increase of water desorption energy from COOH SAM at very low coverage of water [16]. The weak interaction between the composite structure and the water molecules above this composite structure decreased the stabilization of interfacial water on COOH SAM, as found by Raman spectroscopy in comparison with other hydrophilic surfaces, i.e., OH SAM [17]. These results are consistent with the existence of embedded water in the COOH matrix of COOH SAM predicted in the present study.

In summary, using MD simulations and quantum mechanics calculations, we have found that water molecules can be embedded into the COOH matrix on COOH SAMs with appropriate packing densities to form embedded-water–COOH composite structures. The embedded water together with COOH groups maintain an integrated H-bond network within the composite structure, resulting in reduced H-bond formation between the composite structure and water molecules above the composite structure, which explains both the abnormal increase of water desorption energy on COOH SAM when water coverage decreasing even down to 4% [16] and the decreased stabilization of interfacial water on COOH SAM as compared to that on OH SAM [17]. We note that James *et al.* observed the existence of a few-angstrom-thin water layer between water droplets and COOH SAM, and this water layer was spread all over the COOH SAM [14]. We think that their observation can be explained in terms of an embedded-water–COOH composite structure with water droplets. We emphasized that it is only the water molecules themselves that stabilize the COOH structure to form the embedded-water–COOH composite structure. Moreover, the H-bond network of the embedded-water–COOH composite structure makes an "apparent" enhancement of the hydrophobicity of COOH SAM. The relevant contact angles, along with the related stability of the composite structure, were found to exhibit two states, at either ~0° or ~35° in our simulations. This outcome compares favorably to the experimental measurements of contact angles collected from forty research articles (listed in Table S3 of the Supplemental Material [28]); of these, thirty-four observations fall into these two angle ranges that we have predicted.

It is worth noting that composite structures may also exist on many other surfaces with hydrophilic groups, which extends our understanding of the behavior of water on surfaces [87–92], including surfaces on biomolecules. In fact, the coexistence of water droplets and thin water films has been observed on a membrane formed with a bovine serum albumin -Na_2CO_3 mixture [93].

We thank Yi Gao, Guosheng Shi, Rongzheng Wan, Wenpeng Qi, and Jian Liu for their constructive suggestions. This work was supported by the National Natural Science Foundation of China (No. 11290164, No. 11204341), the National Science Fund for Outstanding Young Scholars (No. 11422542), the Youth Innovation Promotion Association CAS, the Key Research Program of Chinese Academy of Sciences (No. KJZD-EW-M03), the Deepcomp7000 and ScGrid of Supercomputing Center, the Computer Network Information Center of Chinese Academy of Sciences and the Shanghai Supercomputer Center of China.

*ystu@yzu.edu.cn
†fanghaiping@sinap.ac.cn

[1] J. C. Love, L. A. Estroff, J. K. Kriebel, R. G. Nuzzo, and G. M. Whitesides, Chem. Rev. **105**, 1103 (2005).

[2] R. C. Major, J. E. Houston, M. J. McGrath, J. I. Siepmann, and X. Y. Zhu, Phys. Rev. Lett. **96**, 177803 (2006).
[3] J. Lahann, S. Mitragotri, T.-N. Tran, H. Kaido, J. Sundaram, I. S. Choi, S. Hoffer, G. A. Somorjai, and R. Langer, Science **299**, 371 (2003).
[4] J. Y. Chen, I. Ratera, J. Y. Park, and M. Salmeron, Phys. Rev. Lett. **96**, 236102 (2006).
[5] Y. Pei and J. Ma, J. Am. Chem. Soc. **127**, 6802 (2005).
[6] S.-W. Lee and P. E. Laibinis, J. Am. Chem. Soc. **122**, 5395 (2000).
[7] M. K. Ferguson, J. R. Lohr, B. S. Day, and J. R. Morris, Phys. Rev. Lett. **92**, 073201 (2004).
[8] C. T. Konek, M. J. Musorrafiti, H. A. Al-Abadleh, P. A. Bertin, S. T. Nguyen, and F. M. Geiger, J. Am. Chem. Soc. **126**, 11754 (2004).
[9] D. Samanta and A. Sarkar, Chem. Soc. Rev. **40**, 2567 (2011).
[10] A. Tu, H. R. Kwag, A. L. Barnette, and S. H. Kim, Langmuir **28**, 15263 (2012).
[11] Y. Arima and H. Iwata, J. Mater. Chem. **17**, 4079 (2007).
[12] S. Choi, Y. Yang, and J. Chae, Biosens. Bioelectron. **24**, 893 (2008).
[13] H. Ohnuki, M. Izumi, S. Lenfant, D. Guerin, T. Imakubo, and D. Vuillaume, Appl. Surf. Sci. **246**, 392 (2005).
[14] M. James, T. A. Darwish, S. Ciampi, S. O. Sylvester, Z. M. Zhang, A. Ng, J. J. Gooding, and T. L. Hanley, Soft Matter **7**, 5309 (2011).
[15] L. H. Dubois, B. R. Zegarski, and R. G. Nuzzo, Proc. Natl. Acad. Sci. U.S.A. **84**, 4739 (1987).
[16] L. H. Dubois, B. R. Zegarski, and R. G. Nuzzo, J. Am. Chem. Soc. **112**, 570 (1990).
[17] D. J. Tiani, H. Yoo, A. Mudalige, and J. E. Pemberton, Langmuir **24**, 13483 (2008).
[18] N. Winter, J. Vieceli, and I. Benjamin, J. Phys. Chem. B **112**, 227 (2008).
[19] Z. Xu, K. Song, S.-L. Yuan, and C.-B. Liu, Langmuir **27**, 8611 (2011).
[20] M. Szori, P. Jedlovszky, and M. Roeselova, Phys. Chem. Chem. Phys. **12**, 4604 (2010).
[21] A. Osnis, C. N. Sukenik, and D. T. Major, J. Phys. Chem. C **116**, 770 (2012).
[22] M. J. Stevens and G. S. Grest, Biointerphases **3**, FC13 (2008).
[23] T. R. Lee, R. I. Carey, H. A. Biebuyck, and G. M. Whitesides, Langmuir **10**, 741 (1994).
[24] K. M. Evans-Nguyen and M. H. Schoenfisch, Langmuir **21**, 1691 (2005).
[25] J. P. Perdew, K. Burke, and M. Ernzerhof, Phys. Rev. Lett. **77**, 3865 (1996).
[26] B. Delley, J. Chem. Phys. **113**, 7756 (2000).
[27] B. Delley, J. Chem. Phys. **92**, 508 (1990).
[28] See Supplemental Material at http://link.aps.org/supplemental/10.1103/PhysRevLett.115.186101 for more detailed methods, data of additional QM calculations, and MD simulations and discussions, and the literature list of experimental contact angles of water droplets on COOH SAMs, which also includes Refs. [29–73].
[29] T. Werder, J. H. Walther, R. L. Jaffe, T. Halicioglu, and P. Koumoutsakos, J. Phys. Chem. B **107**, 1345 (2003).
[30] X. Li, J. Y. Li, M. Eleftheriou, and R. H. Zhou, J. Am. Chem. Soc. **128**, 12439 (2006).
[31] H. Li and X. C. Zeng, ACS Nano **6**, 2401 (2012).
[32] A. Sieval, A. Demirel, J. Nissink, M. Linford, J. Van der Maas, W. De Jeu, H. Zuilhof, and E. Sudhölter, Langmuir **14**, 1759 (1998).
[33] C. D. Bain and G. M. Whitesides, Angew. Chem., Int. Ed. Engl. **28**, 506 (1989).
[34] C. A. Scotchford, C. P. Gilmore, E. Cooper, G. J. Leggett, and S. Downes, J. Biomed. Mater. Res. **59**, 84 (2002).
[35] N. Patel, M. C. Davies, M. Hartshorne, R. J. Heaton, C. J. Roberts, S. J. Tendler, and P. M. Williams, Langmuir **13**, 6485 (1997).
[36] B. D. Beake and G. J. Leggett, Phys. Chem. Chem. Phys. **1**, 3345 (1999).
[37] C. D. Bain, E. B. Troughton, Y. T. Tao, J. Evall, G. M. Whitesides, and R. G. Nuzzo, J. Am. Chem. Soc. **111**, 321 (1989).
[38] C. E. D. Chidsey and D. N. Loiacono, Langmuir **6**, 682 (1990).
[39] J. K. Lee, Y.-G. Kim, Y. S. Chi, W. S. Yun, and I. S. Choi, J. Phys. Chem. B **108**, 7665 (2004).
[40] E. Frydman, H. Cohen, R. Maoz, and J. Sagiv, Langmuir **13**, 5089 (1997).
[41] D. A. Hutt and G. J. Leggett, Langmuir **13**, 2740 (1997).
[42] I. Hirata, M. Akamatsu, E. Fujii, S. Poolthong, and M. Okazaki, Dent. Mater. J. **29**, 438 (2010).
[43] N. Faucheux, R. Tzoneva, M. D. Nagel, and T. Groth, Biomaterials **27**, 234 (2006).
[44] M. A. Hallen and H. D. Hallen, J. Phys. Chem. C **112**, 2086 (2008).
[45] P. F. Driscoll, E. Milkani, C. R. Lambert, and W. G. McGimpsey, Langmuir **26**, 3731 (2010).
[46] C. C. A. Ng, S. Ciampi, J. B. Harper, and J. J. Gooding, Surf. Sci. **604**, 1388 (2010).
[47] E. Cooper, R. Wiggs, D. A. Hutt, L. Parker, G. J. Leggett, and T. L. Parker, J. Mater. Chem. **7**, 435 (1997).
[48] P. G. Ganesan, A. P. Singh, and G. Ramanath, Appl. Phys. Lett. **85**, 579 (2004).
[49] C.-W. Chang and J.-D. Liao, Nanotechnology **19**, 315703 (2008).
[50] H. Wang, S. Chen, L. Li, and S. Jiang, Langmuir **21**, 2633 (2005).
[51] H. S. Ahn, P. D. Cuong, S. Park, Y. W. Kim, and J. C. Lim, Wear **255**, 819 (2003).
[52] Z. Kong, Q. Wang, and L. Ding, Appl. Surf. Sci. **256**, 1372 (2009).
[53] J. Singh and J. E. Whitten, J. Macromol. Sci., Phys. **45**, 884 (2008).
[54] V. A. Tegoulia and S. L. Cooper, Colloids Surf. B. Biointerfaces **24**, 217 (2002).
[55] H. J. Yan, S. Zhang, J. He, Y. B. Yin, X. M. Wang, X. B. Chen, F. Z. Cui, Y. Li, Y. Z. Nie, and W. M. Tian, Biomed. Mater. **8**, 035008 (2013).
[56] K. Konno, E. Ito, J. Noh, and M. Hara, Jpn. J. Appl. Phys. **45**, 405 (2006).
[57] L. Y. Li, S. F. Chen, and S. Y. Jiang, Langmuir **19**, 2974 (2003).
[58] B. G. Keselowsky, D. M. Collard, and A. J. García, J. Biomed, J. Biomed. Mater. Res. **66A**, 247 (2003).

[59] S. Gourianova, N. Willenbacher, and M. Kutschera, Langmuir **21**, 5429 (2005).
[60] S. M. Mendoza, I. Arfaoui, S. Zanarini, F. Paolucci, and P. Rudolf, Langmuir **23**, 582 (2007).
[61] K. E. Michael, V. N. Vernekar, B. G. Keselowsky, J. C. Meredith, R. A. Latour, and A. J. García, Langmuir **19**, 8033 (2003).
[62] M. R. Anderson and R. Baltzersen, J. Colloid Interface Sci. **263**, 516 (2003).
[63] T. Nakaji-Hirabayashi, K. Kato, Y. Arima, and H. Iwata, Biomaterials **28**, 3517 (2007).
[64] K. J. Lee, F. Pan, G. T. Carroll, N. J. Turro, and J. T. Koberstein, Langmuir **20**, 1812 (2004).
[65] H. Xu and B. Berne, J. Phys. Chem. B **105**, 11929 (2001).
[66] J. Zielkiewicz, J. Chem. Phys. **123**, 104501 (2005).
[67] D. Swiatla-Wojcik, Chem. Phys. **342**, 260 (2007).
[68] F. H. Stillinger and A. Rahman, J. Chem. Phys. **60**, 1545 (1974).
[69] A. Kuffel and J. Zielkiewicz, J. Phys. Chem. B **112**, 15503 (2008).
[70] W. L. Jorgensen, J. Chandrasekhar, J. D. Madura, R. W. Impey, and M. L. Klein, J. Chem. Phys. **79**, 926 (1983).
[71] S. Pal, S. Balasubramanian, and B. Bagchi, Phys. Rev. E **67**, 061502 (2003).
[72] S. Balasubramanian, S. Pal, and B. Bagchi, Phys. Rev. Lett. **89**, 115505 (2002).
[73] V. A. Makarov, B. K. Andrews, P. E. Smith, and B. M. Pettitt, Biophys. J. **79**, 2966 (2000).
[74] B. Hess, C. Kutzner, D. van der Spoel, and E. Lindahl, J. Chem. Theory Comput. **4**, 435 (2008).
[75] W. L. Jorgensen, D. S. Maxwell, and J. TiradoRives, J. Am. Chem. Soc. **118**, 11225 (1996).
[76] H. J. C. Berendsen, J. R. Grigera, and T. P. Straatsma, J. Phys. Chem. **91**, 6269 (1987).
[77] U. Essmann, L. Perera, M. L. Berkowitz, T. Darden, H. Lee, and L. G. Pedersen, J. Chem. Phys. **103**, 8577 (1995).
[78] C. L. Wang, H. J. Lu, Z. G. Wang, P. Xiu, B. Zhou, G. H. Zuo, R. Z. Wan, J. Z. Hu, and H. P. Fang, Phys. Rev. Lett. **103**, 137801 (2009).
[79] C. Q. Zhu, H. Li, Y. F. Huang, X. C. Zeng, and S. Meng, Phys. Rev. Lett. **110**, 126101 (2013).
[80] D. T. Limmer, A. P. Willard, P. Madden, and D. Chandler, Proc. Natl. Acad. Sci. U.S.A. **110**, 4200 (2013).
[81] C. L. Wang, B. Zhou, P. Xiu, and H. P. Fang, J. Phys. Chem. C **115**, 3018 (2011).
[82] C. L. Wang, B. Zhou, Y. S. Tu, M. Y. Duan, P. Xiu, J. Y. Li, and H. P. Fang, Sci. Rep. **2**, 358 (2012).
[83] K. Marushkevich, L. Khriachtchev, J. Lundell, A. Domanskaya, and M. Rasanen, J. Phys. Chem. A **114**, 3495 (2010).
[84] P. I. Nagy, Comput. Theor. Chem. **1022**, 59 (2013).
[85] C. H. Gorbitz and M. C. Etter, J. Am. Chem. Soc. **114**, 627 (1992).
[86] P. Ball, Chem. Rev. **108**, 74 (2008).
[87] M. Ahmad, W. Gu, T. Geyer, and V. Helms, Nat. Commun. **2**, 261 (2011).
[88] R. Villey, E. Martinot, C. Cottin-Bizonne, M. Phaner-Goutorbe, L. Leger, F. Restagno, and E. Charlaix, Phys. Rev. Lett. **111**, 215701 (2013).
[89] L. Zhao, C. L. Wang, J. Liu, B. H. Wen, Y. S. Tu, Z. W. Wang, and H. P. Fang, Phys. Rev. Lett. **112**, 078301 (2014).
[90] J. Guo, X. Z. Meng, J. Chen, J. B. Peng, J. M. Sheng, X.-Z. Li, L. M. Xu, J.-R. Shi, E. Wang, and Y. Jiang, Nat. Mater. **13**, 184 (2014).
[91] X. Liu, C. Leng, L. Yu, K. He, L. J. Brown, Z. Chen, J. Cho, and D. Wang, Angew. Chem. **127**, 4933 (2015).
[92] N. Choudhury, J. Chem. Phys. **131**, 014507 (2009).
[93] Y. Wang, Z. G. Duan, and D. D. Fan, Sci. Rep. **3**, 3505 (2013).